Enhancing the dynamic performance of a pantograph-catenary system via inerter-based damping technology

Ming Zhu[1], Sara Ying Zhang[1], Jason Zheng Jiang[1], John Macdonald[1], Simon Neild[1]

[1] Faculty of Engineering, University of Bristol
Queen's Building, University Walk, Bristol, BS8 1TR, UK.
e-mail: **ming.zhu@bristol.ac.uk, yz13229@bristol.ac.uk**,**z.jiang@bristol.ac.uk**,
John.Macdonald@bristol.ac.uk, **Simon.Neild@bristol.ac.uk**.

Abstract

A key aim in designing pantograph-catenary (P-C) systems is to maintain an optimal contact force between the pantograph and catenary cables, which guarantees the power transmission efficiency while minimising wear and damage of the contacting elements. However, with increased operation velocity, undesirable vibrations between the pantograph and the catenary can result in poorer power transmission and load damage. To allow faster travel, advanced vibration suppression techniques for P-C system are needed. Here we consider enhancing the performance by adopting inerter-based damping technologies. A typical time-varying lumped model of a P-C system is considered in this work. Optimal suspension configurations show that up to a 25% reduction in contact force variance can be achieved comparing with a traditional passive system.

1 Introduction

The pantograph-catenary system is the most feasible way to power high-speed trains at present. An uplift mechanism keeps the pantograph current collectors or the panhead in contact with the contact wire. A good contact performance between the pantograph and catenary is the most significant factor for maintaining a stable power supply. The dynamics of the pantograph-catenary system play a crucial role in the current collection quality. As the train's speed increases, the vibrations of the pantograph-catenary system become stronger, which deteriorates the power transmission and accelerates the wear of the contact components [1]. To balance the power transmission behaviour and mechanical wear, a novel pantograph design is needed.

The inerter [2, 3] opens up new possibilities for passive control of mechanical systems. The inerter is a mechanical device with two terminals having the property that the generated force is proportional to the relative acceleration between its terminals. Applications of the inerter to control of motorcycle steering instabilities [4], vehicle suspension [5, 6], buildings [7, 8], railway vehicle suspension [9, 10] and landing gears [11,12] have been identified. The results have shown that the performance of the systems can be significantly improved with the use of inerters. The inerter has been successfully deployed in Formula 1 racing since 2005, under the name of J-damper.

Different mathematical models and simulation methods have been introduced to quantitatively study pantograph-catenary interaction. In these works, the finite element method (FEM) is usually applied to model the catenary system. Andrea et al. [13] built a FEM model of the catenary which applied a procedure based on the penalty method to simulate the contact between wire and collector. Cho et al. [14] proposed both the formulation of a nonlinear dropper and the proper implementation of a time-integration method for the FEM of pantograph–overhead contact line dynamics. A modelling method based on the analytical expressions of nonlinear cable and truss elements was proposed by Yang et al. in [15]. Athough the FEM is accurate, the model is complicated and time-consuming. Hence some simpler catenary models

are also proposed. For example, Wu et al. [16] modeled the catenary system as a time-varying stiffness with a single-degree-of-freedom model of the pantograph.

This paper is structured as follows. In Section 2, the simplified catenary model with lumped time-varying parameters and a two-degree-of-freedom pantograph model are presented. In Section 3, candidate absorber layouts and the optimization procedure are proposed and discussed. The optimisation results and the corresponding time domain responses are shown in section 4. In Section 5, the conclusion is drawn.

2 Modelling of the pantograph-catenary system

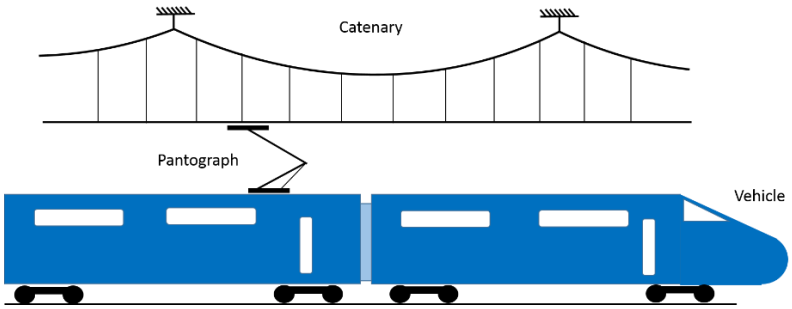

Figure 1: Schematic of pantograph-catenary system.

The pantograph-catenary system shown in Figure 1 is a complicated system which consists of two longitudinal wires connected by some droppers together with a pantograph. A mathematical model of the complete overhead suspension system and the catenary is difficult to define because it is a distributed system. Some FEM models of catenary system have been established, but these models are usually complicated and time-consuming to simulate. Simplified models with lumped time-varying parameters have been shown to be sufficiently accurate for control and design purposes [17]. Here we consider the model from reference [18] in Figure 2, which models the dynamics of the catenary and a two-degree-of-freedom pantograph. The system parameters are shown in Table 1 where m_c, k_c, c_c are the equivalent mechanical parameters of the catenary system, presenting periodic behaviour along each span. Fourier series expressions of equivalent parameters of catenary system including the first, second and third harmonics are applied using [18]

$$\begin{aligned} m_c(t) &= m_{c0} + \sum_{i=1}^{3} m_{ci} \cos\left(\frac{2i\pi}{L} X(t)\right) \\ c_c(t) &= c_{c0} + \sum_{i=1}^{3} c_{ci} \cos\left(\frac{2i\pi}{L} X(t)\right) \\ k_c(t) &= k_{c0} + \sum_{i=1}^{3} k_{ci} \cos\left(\frac{2i\pi}{L} X(t)\right) \end{aligned} \quad , \tag{1}$$

where $X(t)$ is the horizontal distance of the pantograph from a reference tower. The values of m_{ci}, c_{ci} and k_{ci} are given in Table 1. In Figure 2, k_1 and c_1 represent the contact stiffness and damping between panhead and catenary. The remaining parameters care for the two-degree of freedom system modelling the pantograph. During normal operation, the pantograph is always in contact with the catenary, which implies that $x_1 \equiv x_c$ and the contact force $F_c = k_1(x_2 - x_1) + c_1(\dot{x}_2 - \dot{x}_1)$ is nonnegative, where x_c, x_1, x_2 are the displacements of catenary, contact surface and upper frame. It has been checked that this condition always hold in our investigation presented here.

The pantograph is modelled as a two-degree-of-freedom system shown in Figure 2. A linear system can approximate the pantograph dynamics in the vicinity of the working configuration. In the default model, only a damper, represented by c_3, is installed in primary suspension system. For default model, the suspension force F_d in Figure 2 can be presented as

$$F_d = -c_3 \dot{x}_3, \tag{2}$$

where $\dot{x}_3$ is the velocity of lower frame.

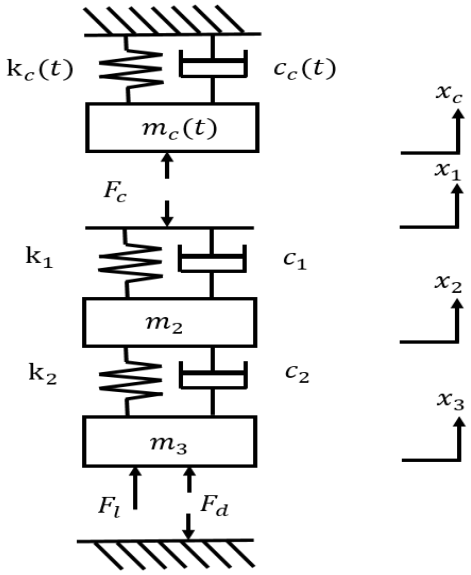

Figure 2: The lumped model of pantograph-catenary system with time-varying parameters.

Parameters	Notation	Value
Lower frame parameters	m_3	9.5 kg
	c_3	5000 Ns/m
Upper frame parameters	m_2	7.6 kg
	c_2	20 Ns/m
	k_2	3421 N/m
Head parameters	c_1	5000 Ns/m
	k_1	10^5 N
Catenary mass parameters	m_{c0}	195 kg
	m_{c1}	100 kg
	m_{c2}	20 kg
	m_{c3}	5 kg
Catenary damping parameters	c_{c0}	240 Ns/m
	c_{c1}	240 Ns/m
	c_{c2}	50 Ns/m
	c_{c3}	12 Ns/m
Catenary stiffness parameters	k_{c0}	7000 N/m
	k_{c1}	3360 N/m
	k_{c2}	650 N/m
	k_{c3}	160 N/m
Span length	L	65.52 m
Uplift force	F_l	100 N

Table 1. Model parameters.

If aerodynamic forces are ignored, the motion of the whole system is governed by

$$\begin{aligned} m_c(t)\ddot{x}_1 &= -k_c(t)x_1 - c_c(t)\dot{x}_1 + k_1(x_2 - x_1) + c_1(\dot{x}_2 - \dot{x}_1) \\ m_2\ddot{x}_2 &= -k_1(x_2 - x_1) - c_1(\dot{x}_2 - \dot{x}_1) + k_2(x_3 - x_2) + c_2(\dot{x}_3 - \dot{x}_2), \\ m_3\ddot{x}_3 &= -k_2(x_3 - x_2) - c_2(\dot{x}_3 - \dot{x}_2) + F_d + F_l \end{aligned} \tag{3}$$

where F_l is the uplift force which is set to be 100 N in this work, same as the value used in [19].

3 Candidate layouts and optimization procedure

Our aim is to redesign primary suspension system between lower frame and base to achieve a better performance of pantograph-catenary system in the range of operation speed. Three candidate layouts (S2, S3, S4 in Figure 3) including 3 elements (one spring, one damper and one inerter) are considered in this paper. The S1 in Figure 3 is the default structure which used in traditional pantograph.

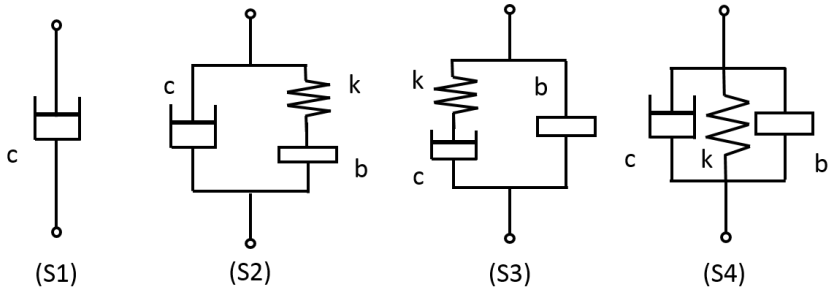

Figure 3: Candidate suspension device layouts.

The transfer functions of proposed candidate layouts are represented by $Y(s) = \frac{F(s)}{V(s)}$, where $F(s)$ and $V(s)$ are the force at the terminals and the relative velocity across the terminals in the Laplace domain. The suspension force F_d can be expressed by

$$F_d = -\mathrm{sY(s)}\tilde{x}_3, \tag{4}$$

where $\tilde{x}_3$ is the displacement of lower frame in the Laplace domain.

A key aim in designing pantograph systems is to maintain an optimal contact force between the pantograph and catenary cables. This force balances the need for satisfactory power transmission and minimum wear and damage of the contacting elements, which is apparent for high-speed trains. The root-mean-square of difference between contact force $F_c(v,t)$ and uplift F_l are calculated to evaluate this performance of the pantograph-catenary system. The performance index function $\delta(v)$ can be definite as

$$\delta(v) = rms(F_c(v,t) - F_l), v \in [20\mathrm{m/s}, 100\mathrm{m/s}]. \tag{5}$$

The cost function in this work is the value of $\delta(v)$ at nominal operation speed v_{op}

$$J = \delta|_{v=v_{op}}. \tag{6}$$

In order to make sure the performances of proposed layouts are not worse than the default one at all speed values considered, a constraint on performance index function is applied,

$$D_\delta(v) = \delta(v)|_{default} - \delta(v)|_{Si} \geq 0, i \in \{1,2,3,4\}, v \in [20\mathrm{m/s}, 100\mathrm{m/s}], \tag{7}$$

where Si represent the candidate layouts.

Apart from this, the maximum pantograph vertical displacement is related to the operation safety of pantograph-catenary system. According to BS EN50367:2012 (Technical criteria for the interaction between pantograph and overhead line), maximum pantograph vertical amplitude should not be bigger than 80 mm, which means vertical displacement of panhead is also a crucial index to be considered. The maximum panhead displacement $d_{max}(v)$ can be calculated as

$$d_{max}(v) = max(d(v,t)), v \in [20\text{m/s}, 100\text{m/s}], \quad (8)$$

where $d(v,t)$ is the time history of the panhead displacement with the operation speed v.

An additional constraint on the maximum panhead displacement is also applied, in the optimisation, which can be definite as

$$D_{\max}(v) = d_{max}(v)|_{default} - d_{max}(v)|_{Si} \geq 0, i \in \{1,2,3,4\}, v \in [20\text{m/s}, 100\text{m/s}]. \quad (9)$$

In the simulation, the nominal operation speed is selected as $v_{op} = 75\ \text{m/s}$ in this work. The 'patternsearch' and 'fminsearch' in MATLAB are used for optimization.

4 Optimization results and discussion

The optimal results with corresponding optimum parameter values for the four layouts are shown in Table 2.

No.	Structure parameters			Performance	
	b (kg)	c (Ns/m)	k (N/m)	J (N)	d_{max} (mm)
default	/	5000	/	55(-)	44
S1	/	5000	/	55(0%)	44
S2	3.16	2061	154	42(23%)	37
S3	0.03	2211	32715	41(25%)	39
S4	10.00	2126	301	42(23%)	37

Table 2: The optimization results and the optimum parameter values.

From Table 2, the optimal value of S1 is the same as the default one where $c_3 = 5000\ \text{Ns/m}$. In order to explain this phenomenon, a sensitivity analysis of S1 is carried out. Take $c_3 = 2000\ \text{Ns/m}$ as an example. The constraints values of $D_\delta(v)$ and $D_{\max}(v)$ are calculated as

$$D_\delta(v) = \delta(v)|_{default, c_3=5000} - \delta(v)|_{S1, c_3=2000}, \quad (10)$$

$$D_{\max}(v) = d_{max}(v)|_{default, c_3=5000} - d_{max}(v)|_{S1, c_3=2000}. \quad (11)$$

From Figure 4(a), D_δ is bigger than 0 in the whole speed sector, which satisfies the constraint on performance index function. From Figure 4(b), $D_{\max}$ is smaller than 0 between 0 m/s to about 35 m/s and between about 45 m/s to 60 m/s, which means the constraint on maximum panhead displacement is not satisfied when $c_3 = 2000\ \text{Ns/m}$.

For the parameter c_3 varying from 0 to 10000 Ns/m, the contours of D_δ and $D_{\max}$ can be gained on the c_3-velocity plane as shown in Figure 5. Figure 5(a) is the contours of D_δ on the c_3-velocity plane. The colourful region means $D_\delta > 0$, which satisfies the constraint of performance index function. If we cut through the solid red in Figure 5(a), the cross section is shown as Figure 4(a). Figure 5(b) is the contours of $D_{\max}$ on the c_3- velocity plane. The colourful region means $D_{\max}$ is bigger than zero which satisfies the constraint of the maximum panhead displacement. Similarly, the Figure 4(b) is also the cross section if we cut through the solid red in Figure 5(b).

From Figure 5(a), when we decrease the value of c_3, the constraint on performance index function can be satisfied in the whole range of operation speed. From Figure 5(b), larger value of c_3 can satisfy the constraint on the maximum panhead displacement at low speed (between about 0 to 35 m/s) while smaller value of c_3 can satisfies the constraint on the maximum panhead displacement at high speed (between about 70 to 100 m/s). Above all, if structure S1 is applied in the primary suspension, we can't find a better value of c_3 to achieve better performance while satisfying the two constraints at the same time.

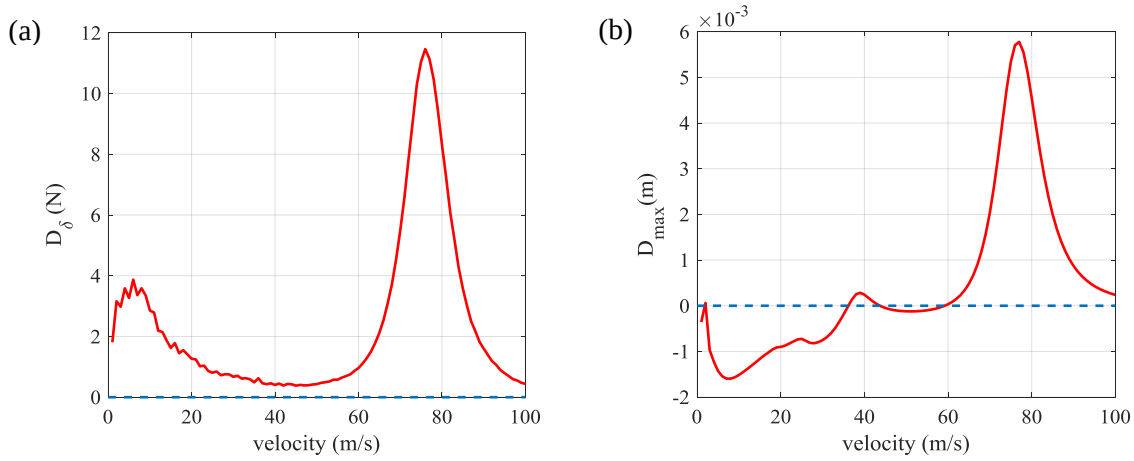

Figure 4: (a) Difference of performance index function $\delta(v)$ in velocity domain between $c_3 = 5000$ Ns/m and 2000 Ns/m; (b) Difference of maximum panhead displacement in velocity domain between $c_3 = 5000$ Ns/m and 2000 Ns/m.

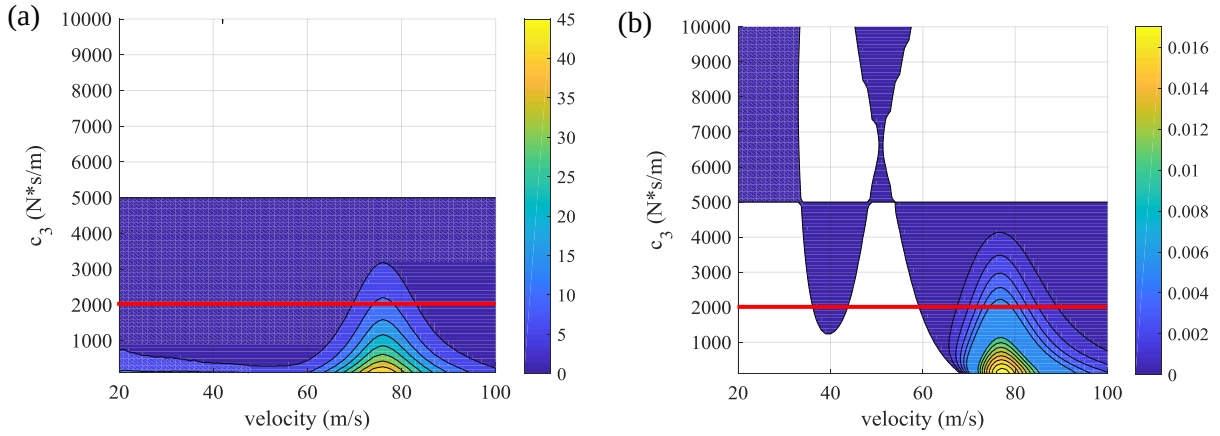

Figure 5: (a) The contours of D_δ, (b) The contours of D_{max}.

It can be also seen from Table 2, the proposed three inerter-based structures (S2, S3, S4) can provide significant performance improvement, with up to 25%. The corresponding results are shown in Figure 6. Figure 6(a) suggests that all the proposed configurations (S2, S3, S4) satisfy the two constraints. According to Table 2, the S3 gain the largest improvement (25%) in the proposed cost function *J* while its maximum panhead displacement is higher than that of S2 and S4. The performance of S2 and S4, both with 23% improvement, are very similar to each other.

It can be seen that the maximum panhead displacement of S2 and S4 (37 mm) is smaller than that of S3 (39 mm), which shows better performance on operation safety.

The responses in time domain are also analyzed to validate the optimization results. The responses in time-domain of the whole system are harmonic because the whole system is harmonic parametric self-excited system. The responses at operation speed of 75 m/s (between 28 s and 30 s) are shown on Figure 7. From Figure 7(a), the contact forces oscillate around 100 N. The variance of contact forces of inerter-based configurations S2, S3, S4 are significantly smaller than S1, which is consistent with the result shown on Table 2. It can be seen from Figure 7(b), the maximum panhead displacements of inert-based configurations are also smaller than default one, which verify the maximum panhead displacement constraint. It also can be noted that the maximum panhead displacement of S3 is larger than S2 and S4 in time domain as is obtained in Figure 6.

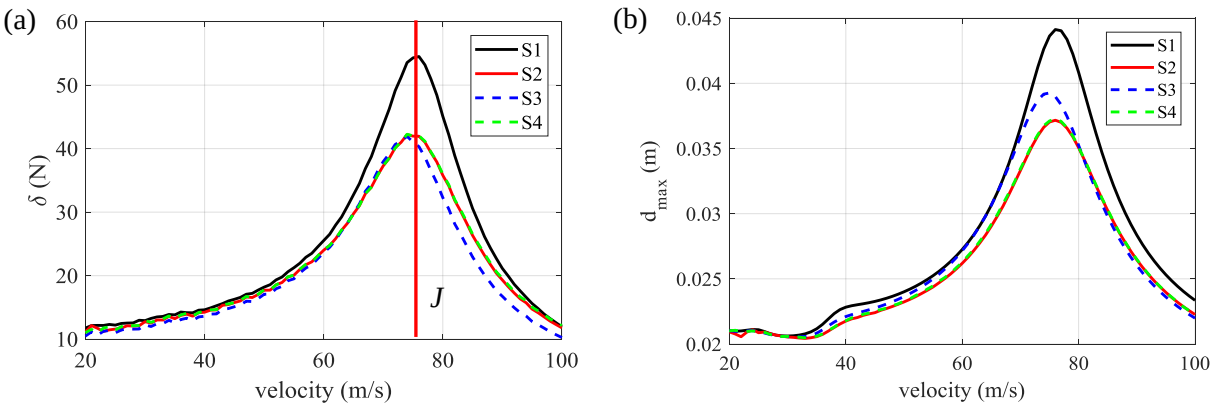

Figure 6: The $\delta(v)$ and $d_{max}(v)$ of different candidate layouts with velocity from 20 m/s to 100 m/s.

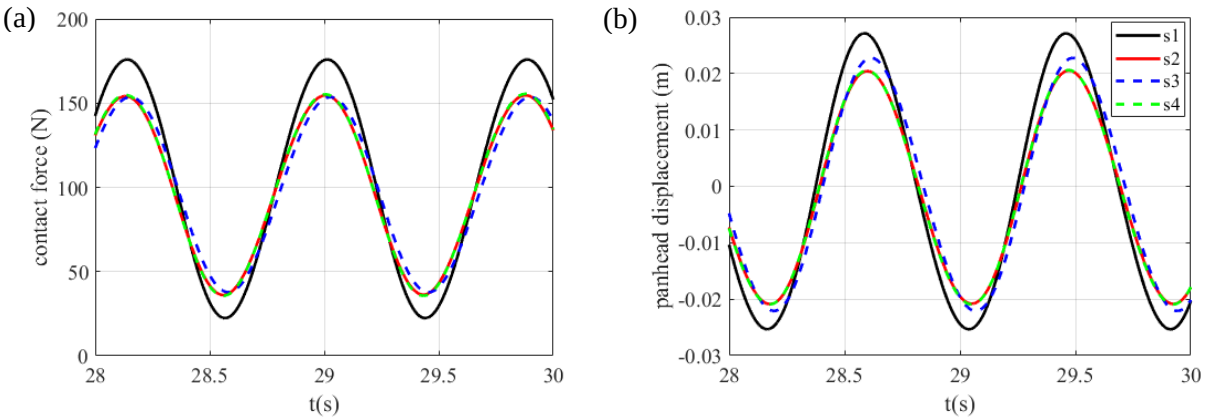

Figure 7: Response in time domain: (a) contact forces of S1, S2, S3, S4 in time domain; (b) Panhead displacement of S1, S2, S3, S4 in time domain.

5 Conclusion

The inerter-based vibration suppression technology is applied in pantograph-catenary system in this paper. Three different candidate layouts consisting of one inerter, one damper and one spring are discussed. It has been shown that the inerter-based devices can significantly improve the performance in contact force and reduce the maximum panhead displacement at the same time, which can't be achieved by the traditional primary absorber. Inerter-based device shows huge application prospects to increase the reliability and reduce the maintenance cost of pantograph-catenary system by effectively suppressing the vibration.

6 Acknowledgements

The authors would like to acknowledge the support of the EPSRC, the University of Bristol and the China Scholarship Council. Ming Zhu is supported by the joint scholarship of University of Bristol and the China Scholarship Council; Sara Ying Zhang, Jason Zheng Jiang are supported by the EPSRC grant EP/P013546/1 and Royal Society IE151194; Simon Neild is supported by EPSRC fellowship EP/K005375/1.

Reference

[1] Poetsch, G., EVANS, J., Meisinger, R., Kortüm, W., Baldauf, W., Veitl, A., & Wallaschek, J. (1997). *Pantograph/catenary dynamics and control*. Vehicle system dynamics, 28(2-3), 159-195.

[2] Smith, M. C. (2002). *Synthesis of mechanical networks: The inerter*. IEEE Transactions on automatic control, 47(10), 1648-1662.

[3] Firestone, F. A. (1933). *A new analogy between mechanical and electrical systems*. The Journal of the Acoustical Society of America, 4(3), 249-267.

[4] Evangelou, S., Limebeer, D. J., Sharp, R. S., & Smith, M. C. (2006). *Control of motorcycle steering instabilities*. IEEE control systems, 26(5), 78-88.

[5] Papageorgiou, C., & Smith, M. C. (2006). *Positive real synthesis using matrix inequalities for mechanical networks: application to vehicle suspension*. IEEE Transactions on Control Systems Technology, 14(3), 423-435.

[6] Smith, M. C., & Wang, F. C. (2004). *Performance benefits in passive vehicle suspensions employing inerters*. Vehicle system dynamics, 42(4), 235-257.

[7] Zhang, S. Y., Jiang, J. Z., & Neild, S. (2017). *Optimal configurations for a linear vibration suppression device in a multi-storey building*. Structural Control and Health Monitoring, 24(3).

[8] Lazar, I. F., Neild, S. A., & Wagg, D. J. (2014). *Using an inerter-based device for structural vibration suppression*. Earthquake Engineering & Structural Dynamics, 43(8), 1129-1147.

[9] Wang, F. C., & Liao, M. K. (2010). *The lateral stability of train suspension systems employing inerters*. Vehicle System Dynamics, 48(5), 619-643.

[10] Jiang, J. Z., Matamoros-Sanchez, A. Z., Goodall, R. M., & Smith, M. C. (2012). *Passive suspensions incorporating inerters for railway vehicles*. Vehicle System Dynamics, 50(sup1), 263-276.

[11] Li, Y., Howcroft, C., Neild, S. A., & Jiang, J. Z. (2017). *Using continuation analysis to identify shimmy-suppression devices for an aircraft main landing gear*. Journal of Sound and Vibration, *408*, 234-251.

[12] Li, Y., Jiang, J. Z., Neild, S. A., & Wang, H. (2017). *Optimal Inerter-Based Shock–Strut Configurations for Landing-Gear Touchdown Performance*. Journal of Aircraft, 1-9.

[13] Collina, A., & Bruni, S. (2002). *Numerical simulation of pantograph-overhead equipment interaction*. Vehicle System Dynamics, 38(4), 261-291.

[14] Cho, Y. H. (2008). *Numerical simulation of the dynamic responses of railway overhead contact lines to a moving pantograph, considering a nonlinear dropper*. Journal of sound and vibration, 315(3), 433-454.

[15] Song, Y., Liu, Z., Wang, H., Lu, X., & Zhang, J. (2015). *Nonlinear modelling of high-speed catenary based on analytical expressions of cable and truss elements*. Vehicle System Dynamics, 53(10), 1455-1479.

[16] Wu, T. X., & Brennan, M. J. (1998). *Basic analytical study of pantograph-catenary system dynamics*. Vehicle System Dynamics, 30(6), 443-456.

[17] Allotta, B., Papi, R., Pugi, L., Toni, P., & Violi, A. G. (2001, July). *Experimental campaign on a servo-actuated pantograph*. In Advanced Intelligent Mechatronics, 2001. Proceedings. 2001 IEEE/ASME International Conference on (Vol. 1, pp. 237-242). IEEE.

[18] Pisano, A., & Usai, E. (2008). *Contact force regulation in wire-actuated pantographs via variable structure control and frequency-domain techniques*. International Journal of Control, 81(11), 1747-1762.

[19] Balestrino, A., Bruno, O., Landi, A., & Sani, L. (2000). *Innovative solutions for overhead catenary-pantograph system: wire actuated control and observed contact force*. Vehicle System Dynamics, 33(2), 69-89.